Biosensors and Bioelectronics 151 (2020) 111993

Contents lists available at ScienceDirect

Biosensors and Bioelectronics

journal homepage: http://www.elsevier.com/locate/bios

Early stage detection of *Staphylococcus epidermidis* biofilm formation using MgZnO dual-gate TFT biosensor

Guangyuan Li [a], Yifan Wu [a], Yuxuan Li [a], Yuzhi Hong [b], Xilin Zhao [b], Pavel Ivanoff Reyes [a,*], Yicheng Lu [a,**]

[a] Department of Electrical and Computer Engineering, Rutgers University, Piscataway, NJ, 08854-8058, United States
[b] Public Health Research Institute and Department of Microbiology, Biochemistry & Molecular Genetics, New Jersey Medical School, Rutgers University, Newark, NJ, 07103-3535, United States

ARTICLE INFO

Keywords:
Bioelectric effect
Biofilm detection
Biosensor
Magnesium zinc oxide
Nanostructures
Thin film transistor

ABSTRACT

Early stage detection of biofilm formation is an important aspect of microbial research because once formed, biofilms show serious tolerance to antibiotics in contrast to the free-floating bacteria, which significantly increases the difficulty for clinical treatment of bacterial infections. The early stage detection technology is desired to improve the efficiency of medical treatments. In this work, we present a biosensor consisting of a magnesium zinc oxide (MZO) dual gate thin-film transistor (DGTFT) as the actuator and an MZO nanostructure (MZO_{nano}) array coated conducting pad as the extended sensing gate for the early stage detection of *Staphylococcus epidermidis* (*S. epidermidis*) biofilm formation. *S. epidermidis* bacteria were cultured *in vitro* on the nanostructure modified sensing pad. Charge transfer occurs between microbial cells and the MZO_{nano} during the initial bacterial adhesion stage. Such electrical signals, which represent the onset of biofilm formation, were dynamically detected by the DGTFT where the top gate electrode was connected to the extended MZO_{nano} sensing pad and the bottom gate was used for biasing the device into the optimum characteristic region for high sensitivity and stable operation. The testing results show that a current change of ~80% is achieved after ~200 min of bacterial culturing. A crystal violet staining-based assay shows that tiny bacterial microcolonies just start to form at 200 min, and that it would take approximately 24 h to form matured biofilms. This technology enables medical professionals to act promptly on bacterial infection before biofilms get fully established.

1. Introduction

The worldwide market of biomedical devices, which includes medical indwelling implants, has been growing rapidly in the past few decades and reached $300 billion per year (International Trade Administration, 2016). However, the medical implant technology has been limited by patient tissue rejection and incompatibility due to microbial infections from biofilm formation. In the United States alone, every year approximately 1 million device-associated infections happen due to the bacterial adhesion and the subsequent biofilm formation, resulting in additional medical expense of over $5 billion (Bryers, 2008; Van Epps and Younger, 2016). Although aseptic and sterilization precautions are used, indwelling devices present suitable conditions for free floating bacteria to attach to their surfaces (Khatoon et al., 2018). As the division of bacterial cells and the production of extracellular polymeric substances (EPSs) occur, bacterial microcolonies form at the sites of infection and then eventually develop into matured biofilms (Hall-Stoodley et al., 2004). EPS houses the microbes and offers a unique biochemical environment for them. Once biofilms are established, the conventional antibiotics therapies are largely ineffective since biofilms are characterized to show from 500 to 5000 times more resistant to antibiotic agents than free-floating bacteria of the same kind (Del Pozo et al., 2009). This is mainly because the EPS acts as a protecting layer against the diffusion of antibiotic agents.

The conventional approaches such as phase-contrast microscopy, confocal laser scanning microscopy (CLSM), and biofilm disruption methods combined with staining assays have been employed to visualize and detect bacterial cells and biofilms (Norton et al., 1998; Peeters et al., 2008). However, these techniques are highly labor intensive and very slow. To minimize or even prevent the bacterial infection on medical

* Corresponding author.
** Corresponding author.
E-mail addresses: pavelrey@scarletmail.rutgers.edu (P.I. Reyes), ylu@soe.rutgers.edu (Y. Lu).

https://doi.org/10.1016/j.bios.2019.111993
Received 27 September 2019; Received in revised form 4 December 2019; Accepted 23 December 2019
Available online 28 December 2019
0956-5663/

indwelling devices, a need has emerged for high-throughput analysis and techniques that allow for the early stage detection and monitoring of the biofilm development in real time. In addition, bacterial cells are yet encapsulated in EPS at the early stage of biofilms formation; therefore, antimicrobial agents are still effective to kill the bacteria. As a result, the sooner an infection is detected, the more effective treatment will be. Thus, the development of an early stage biofilm detection technology with high sensitivity and fast response is critically important for timely clinical treatment of bacterial infections.

Two major types of dynamic sensors have been developed to alleviate the limitations of the conventional methods in detection and evaluation of the biofilm formation. These are namely the mass-based sensors (Chen et al., 2010; Kim et al., 2016, 2012) and the electrical impedance sensors (EISs) (Astorga et al., 2019; Becerro et al., 2016; Liu et al., 2018; Paredes et al., 2014b; Paredes et al., 2014a; Paredes et al., 2013, 2012; Pires et al., 2013). The mass-based sensors are capable of precisely measuring the mass accumulation on its surface using acoustic wave devices, including the surface acoustic wave (SAW) sensors and the quartz crystal microbalances (QCMs). Nanogram ranges of mass change can be easily detected by these devices in online and real time modes. Recently, Y. W. Kim et al. demonstrated aluminum oxide (Al_2O_3) passivated ZnO thin film SAW sensor to detect the biofilm formation (Kim et al., 2012) and biofilm removal through bioelectric effect (Kim et al., 2016). On the other hand, the QCM technique was employed to identify the sequence of events occurring in the biofilm formation process and probed the time response under different environmental conditions (Chen et al., 2010). However, both SAW and QCM sensors have been mainly used for monitoring the long-term behavior of biofilm formation because they are intrinsically limited by the sensitivity, i.e. the smallest mass these sensors can detect. The EIS involves the changes in resistance and reactance of the device due to the modulation of the charges on the sensing area introduced by the bacterial cell attachment and biofilm formation. Several works were reported utilizing the detection of impedance variations caused by different phases of biofilm formation (Astorga et al., 2019; Becerro et al., 2016; Liu et al., 2018; Paredes et al., 2014b; Paredes et al., 2014a; Paredes et al., 2013, 2012; Pires et al., 2013). Among them, some effort was made to employ the impedance measurement in different experimental setups mimicking real field environment of bacterial biofilm cultures (Paredes et al., 2014b). The EIS is primarily used for the long-term monitoring of biofilm development on the devices, however there have been some works reporting the detection of early stage biofilm formation by (Astorga et al., 2019; Liu et al., 2018; Paredes et al., 2014a; Pires et al., 2013). These reports all involved EIS as the mechanism for detection combined with various electrode configurations and materials. However, the passive nature of two-terminal electrical impedance devices still limits the sensitivity because of the lack of signal gain. To further enhance the detection sensitivity, which is especially needed for the early stage detection of biofilm formation, a transistor type of three-terminal active device with high signal gain is desired to offer intrinsic amplification to the sensor signals.

ZnO and its related alloys such as MZO are wide bandgap semiconductors which can be made as multifunctional materials through proper doping. ZnO-based nanostructures are known to be biocompatible functional nanostructures used in biosensor technologies (Lu et al., 2011). ZnO nanostructures (ZnO_{nano}) can be grown with various surface morphologies (Cao et al., 2012) on different substrates, including glass and metal electrode surface. The controls of morphology and wettability of ZnO_{nano} were achieved to improve selectivity and sensitivity of biosensors (Taratula et al., 2006; Zhang et al., 2007a). A small percentage of Mg composition is introduced into ZnO to form the ternary compound $Mg_xZn_{1-x}O$ (MZO). MZO keeps the main advantages of the pure ZnO but is able to sustain a larger pH range, which is particularly suitable for the bio-testing process comparing with pure ZnO (Taratula et al., 2006). In addition, ZnO_{nano} would release Zn^{2+} ions into aqueous solutions such as cell culture medium, and the Zn^{2+} ions are toxic to bacteria. In contrast, MZO_{nano} could effectively reduce the toxicity by suppressing the Zn^{2+} ions (Nel et al., 2009; Reyes et al., 2017). Owing to the above advantages, ZnO and MZO have been demonstrated for high sensitivity and compatibility with various biochemicals such as DNA, oligonucleotides, antibodies, proteins, as well as live biological species such as mammalian cells and bacterial strains (Reyes et al., 2017, 2013, 2011, 2009).

ZnO has also been widely employed in thin-film transistors (TFTs) as the active channel layer, due to its high electron mobility, transparent to visible light, and low-cost properties. In 2011, Pavel et al. reported a ZnO bioTFT immunosensor for the detection of EGFR antigen-antibody interaction (Reyes et al., 2011). The ZnO TFT device possessed excellent and repeatable characteristics with a $\sim 10^8$ on-off ratio which provided high sensitivity of the device to the charge modulation within the ZnO channel. The top channel surface of the bioTFT was functionalized with amine-terminated EGFR mAbs as linkers which selectively bond with EGFR proteins. However, it has been shown that when implemented with dual gate structures, TFTs have an additional dimension of control and hence provide more flexibilities in sensing applications (Seok et al., 2013, 2011).

The DGTFT is comprised of a secondary gate electrode and its dielectric layer in addition to the single gate structure of regular TFTs. Much effort has been devoted to developing DGTFTs for various applications, including pixel driving circuits (Baek et al., 2011; Tai et al., 2012b), logic circuits (Seok et al., 2013, 2011; Spijkman et al., 2008), and sensors (Tai et al., 2012a). The operation conditions of DGTFT can be preferably set by the primary gate biasing voltage, while at the same time the secondary gate electrostatically modifies the carrier distribution in the channel accumulated by the primary gate and hence influences the electrical characteristics of the device. This unique feature of DGTFT is exceptionally suitable for biosensing applications.

In this paper, we demonstrate a biosensor consisting of an MZO DGTFT with an MZO_{nano} modified sensing pad as the extended gate for the early stage detection of *S. epidermidis* biofilm formation. Due to the nature of oxide semiconductors, pure ZnO suffers from thermal instability and negative bias stress instability. A small amount of Mg was doped into ZnO to form ternary MZO as the TFT channel material, which suppresses the oxygen vacancy in the active channel benefit from the stronger Mg–O bonding (Ku et al., 2011, 2015). The charge transfer between the microbial cells and the MZO_{nano} during the initial bacterial adhesion stage sends the signals of the onset of biofilm formation into the top gate of DGTFT. *S. epidermidis* was chosen as an example for our study because it is a common cause of infections associated with prosthetic devices and indwelling catheters, such as heart valves, pacemakers, orthopedic implants, and Hickman catheters. *S. epidermidis* is also a frequent infectious agent in many non-biomaterial-related infections including peritonitis, neonatal sepsis, and native valve endocarditis (Kiers et al., 2001). Compared to mass-based sensors, the MZO DGTFT promises to be more sensitive to provide details during the early bacterial adhesion stage, thus enables to predict the subsequent biofilm formation. In comparison with the EIS, the MZO DGTFT transducer intrinsically has high gain due to its field-effect transistor configuration over the two-terminal passive devices. The MZO DGTFT requires significantly lower number of bacterial cells to register a signal due to its high sensitivity, which is needed for the early stage detection of biofilm formation. Moreover, bacterial growth including biofilm formation can be affected by electric fields (Kim et al., 2016) especially if the bacterial samples are placed directly on the active sensing device. Our MZO DGTFT avoids such a problem because its sensing area is the extended MZO_{nano} pad; hence the charge variation caused by the onset of biofilms acts as the biasing voltage on the top gate of the DGTFT. The extended sensing pad design allows the separation of TFT device from the harsh biochemical environment and different sensing pads according to the detection tasks can be connected to the transducer sequentially, which fuels the realization of a plug-in-card type of biosensor. Moreover, the separated sensing pad can be freely modified based on specific

biomolecules to achieve high sensitivity.

This MZO DGTFT biosensor has successfully demonstrated the early stage detection of *S. epidermidis* biofilm formation by choosing the optimized operation point and sensing material. The early stage detection of this work is achieved by focusing the detection on bacterial adhesion stage of biofilm formation. Used in conjunction with other biosensors that are sensitive to the long-term biofilm growth stage discussed earlier, would form a complementary biosensor of studying the complete mechanism of biofilm formation and potential treatment. This MZO DGTFT biosensor can also be adapted to a wide variety of potential scenarios where electrochemical interactions occur, and *in vitro* early stage detection are required.

2. Materials and methods

2.1. MZO DGTFT biosensor

The experimental setup of the MZO DGTFT biosensor is shown in Fig. 1(a). The biosensor consists of two parts: (1) an MZO DGTFT as the signal transducer, and (2) a MZO nanostrcuture modified sensing pad as the biological receptor. Fig. 1(b) and (c) present the cross-sectional and top view of the MZO DGTFT, respectively. In DGTFT, the bottom gate is used as the biasing gate which serves to optimize the operation point, whereas the top gate is used as the sensing gate which is connected to the extended sensing pad. While the bacterial cells adhere themselves onto the sensing pad surface, the electrochemical interactions make a certain portion of cell surface charge transfer downwards to the supporting substratum. Then the transferred charges induce a micro-bias to the top gate and impact the channel current through the field-effect. Thus, the onset of biofilm formation can be monitored. The dual gate design allows the TFT device to perform at the optimum biasing region to achieve the best sensitivity and to ensure the stable operation.

2.1.1. Fabrication of MZO DGTFT

A 50-nm-thick Cr layer was first deposited using electron beam evaporation and then patterned using the standard photolithographic method to form the bottom gate electrode on a glass substrate. Then a SiO_2 film (100 nm) was deposited on top of the Cr bottom gate as the gate dielectric layer using plasma enhanced chemical vapor deposition (PECVD). A 5 nm MgO interfacial layer followed by a 40 nm $Mg_{0.03}Zn_{0.97}O$ channel layer was deposited using metal organic chemical vapor deposition (MOCVD) at ~400 °C, to form a SiO_2/MgO/MZO structure. The ultra-thin MgO layer acts as a barrier to minimize the Zn^{2+} ions diffusion into the SiO_2 dielectric layer, in order to enhance the TFT characteristics and stability (Hong et al., 2016; Li et al., 2018). In MOCVD, DeZn (Diethylzinc), MCp_2Mg (bis-(methyl-cyclopentadienyl) magnesium), and ultra-high purity (99.999%) oxygen gas were used as the Zn metalorganic source, Mg metalorganic source, and oxidizer, respectively. The active mesa area (W/L = 160 μm/15 μm) was formed through wet etching. The source and drain contacts were formed through metallization process (85 nm Ti/35 nm Au/5 nm Ti) followed by a normal lift-off process. Then the top SiO_2 dielectric layer (70 nm) was deposited by PECVD again. Next, a 150-nm-thick Al layer was deposited by electron beam evaporator as the top gate electrode and then patterned. Finally, VIA openings were made using buffered oxide etch solution.

2.1.2. Fabrication of ZnO_{nano} and MZO_{nano} sensing pad

In this biosensor, the ZnO_{nano} or MZO_{nano} pad is used as the extended sensing gate, which is connected to the top gate of DGTFT device. The nanostructured surface is designed due to its giant effective sensing area which enables high sensitivity. The fabrication started from depositing a 5 nm Cr/50 nm Au metal layer using electron beam evaporation process on glass substrate, which serves as the conducting electrode. The metal layer was then patterned and wet etched to form squares of 120 mm^2. The interface between biological materials and the micro-electronics is a key aspect to achieve high sensitivity. For comparisons, 400-nm-thick ZnO and $Mg_xZn_{1-x}O$ nanostructured films (ZnO_{nano} and MZO_{nano}) were grown on the Cr/Au coated glass pad using MOCVD at ~500 °C (Muthukumar et al., 2003). Same precursors and oxidizer as the channel

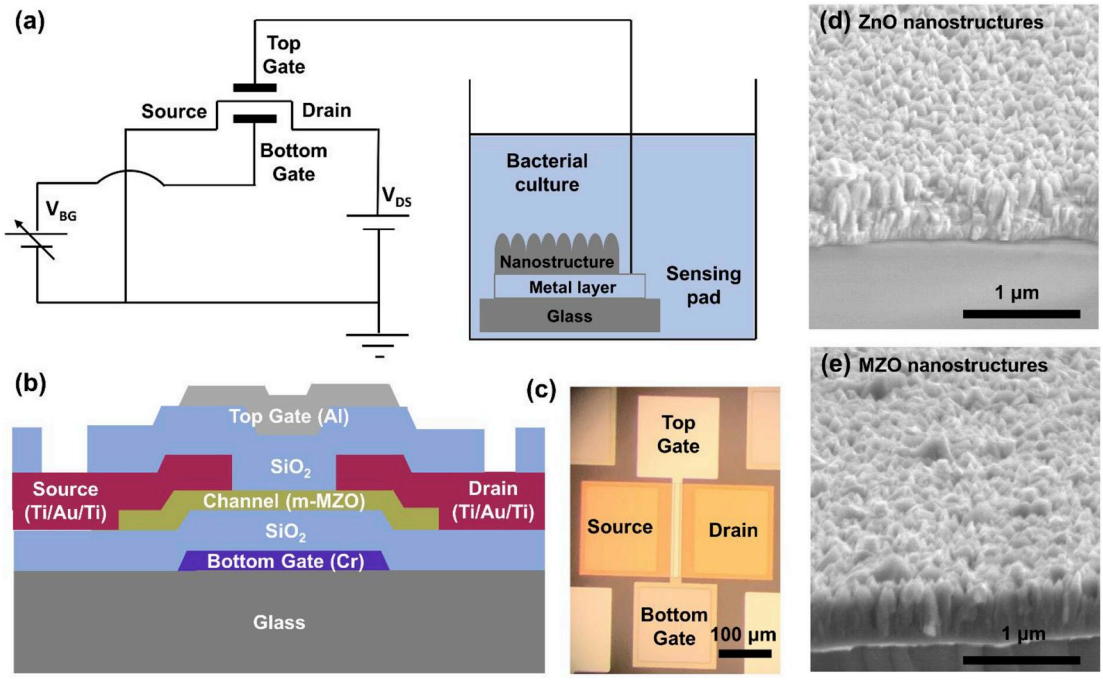

Fig. 1. (a) The experimental setup of the MZO DGTFT biosensor. The biosensor consists of two parts: an MZO DGTFT as the transducer and a ZnO_{nano} or MZO_{nano} modified sensing pad as the receptor. (b) The cross-sectional view of the DGTFT, where the m-MZO presents the combination of the ultra-thin MgO diffusion barrier and the MZO active channel layer. (c) The optical microscope top view of the DGTFT. Four terminals (bottom gate, top gate, source and drain) are labeled accordingly. SEM images of the MOCVD-grown (d) ZnO_{nano} and (e) MZO_{nano} films.

layer were used, however, the x value in $Mg_xZn_{1-x}O$ nanostructures was kept at ~0.04 to enhance the etching resistance, reduce the diffusion of Zn^{2+} ions into the incubation solution and hence reduce the toxicity to the bacterial cells. The scanning electron microscope (SEM) images of the ZnO_{nano} and MZO_{nano} films are shown in Fig. 1(d) and (e), respectively. The roughness of the surface ensures the biosensor with high sensitivity (Reyes et al., 2017). The nanostructured layer was then patterned and wet etched, while leaving a small area of the metal pad open for electrical contact. Then the MZO_{nano} sensing pads underwent UV illumination to get the super-hydrophilic characteristics in order to achieve high sensitivity and minimize the bio-sample consumption (Zhang et al., 2007a,b). The resulting MZO_{nano} and ZnO_{nano} sensing pads possess optimized morphology and wettability, which leads to higher sensitivity of the device.

ZnO and MZO films were then respectively grown on glass substrates to experimentally characterize the x value in $Mg_xZn_{1-x}O$ using the optical absorption measurement. The absorption spectra of ZnO and MZO films were acquired at room temperature by use of a Beckman DU 530 UV–visible spectrometer.

2.2. Biological sample preparation and protocols

2.2.1. Bacterial biofilm incubation

S. epidermidis ATCC 35984 was inoculated into Tryptic Soy Broth (TSB; Becton Dickinson) and then grown at 37 °C for 16–18 h with shaking at 200 rpm. The pH of the culture medium is 7.4 which is close to neutral when prepared according to the manufacturer's prescription. The stationary phase cultures were diluted 100-fold into fresh TSB medium pre-loaded in 10 cm quad-plate Petri dish, with each sector containing 5 mL cultures. The MZO_{nano} and ZnO_{nano} sensing pads were sterilized and placed into the bacterial cultures, with the sensing area being up to allow bacterial adhesion. With the increase of culture time, the bacteria would adhere to the sensing surface first, followed by bacterial expansion and biofilm maturation.

2.2.2. Crystal violet staining assay

The same procedure was followed as describe in Section 2.1.1 but adding one more sensing pad incubated in TSB medium without bacteria as a control. The dishes were incubated statically at 37 °C for biofilm formation. After incubation for 100 min, 200 min, 8 h, 16 h and 24 h, the sensing pads from the cultures were washed three times with 5 mL 0.9% NaCl to remove planktonic cells. Biofilms attached on the sensing surface were then stained using 0.2% crystal violet for 10 min, followed by washing three times with 0.9% NaCl. 100 μL of 30% ethanol was added to each sensing pad to release bound crystal violet when the crystal violet staining solution was removed. The absorbance value was measured at 590 nm using absorption plate reader.

2.3. Electrical measurements and parameters extraction

The MZO DGTFT was placed inside a light-tight measurement station. Its three terminals, i.e. source, drain, and bottom gate were electrically connected to the semiconductor parameter analyzer HP-4156C. A bottom gate biasing voltage V_{BG} was swept between −5 V to 15 V for finding the optimized operation point of the MZO DGTFT. The drain was set at 0.1 V whereas the source was grounded. The drain-source voltage V_{DS} acts as a pump to drive current across the channel. The top sensing gate of the DGTFT was connected to the MZO_{nano} or ZnO_{nano} sensing pad outside of the measurement station. With the increasing of culture time, bacteria adhere themselves onto the MZO_{nano} or ZnO_{nano} sensing pad. This interaction process generates the charge transfer downwards, resulting in a micro-bias applied on the top gate of the DGTFT.

The threshold voltage V_{TH} of the device was extracted using the linear fitting method for 10%–90% of the maximum drain current. The subthreshold slope S.S. value is extracted from a 3-decade range in the subthreshold region ($I_D = 10^{-12}$–10^{-9} A) of the transfer characteristics in logarithm scale.

3. Results and discussion

3.1. Electrical characterization of the MZO DGTFT for biosensor operation

Before we utilize the MZO DGTFT biosensor to dynamically monitor the formation of *S. epidermidis* biofilms, we need to determine three aspects, i.e. the electrical characteristics of the MZO DGTFT without bioreaction, the change of the electrical characteristics during growth of *S. epidermidis* on the extended sensing gate, and the proper biasing voltage on the bottom gate of DGTFT to attain the best combination of high sensitivity and stable operation. The MZO DGTFT biosensor was initially tested by fixing the drain voltage at 0.1 V and sweeping the bottom gate voltage from −5 V to 15 V while the top gate was connected to the extended MZO_{nano} sensing pad that was immersed in TSB medium and let the signal stabilize to baseline value. *S. epidermidis* bacterial culture solution of predetermined volume (see Section 2.2.1) was introduced into the sensing pad with TSB medium at time t = 0 min and let the device incubate for biofilm formation. The transistor transconductance plot (i.e. I–V curves of drain current vs bottom gate bias voltage) were recorded at times t = 0, 50, 125, 200, and 375 min of incubation time. Fig. 2 shows the electrical transfer characteristics of the MZO DGTFT during *S. epidermidis* growth in TSB media. The curve at t = 0 min shows the threshold voltage of 8.4 V, subthreshold swing of 510 mV/dec, and on-off ratio of ~10^8. The steep slope (small value of subthreshold swing), and high on-off ratio indicate high signal gain, therefore high sensitivity of the biosensor.

From the I–V curves in Fig. 2, the drain current dramatically decreases as incubation time increases from t = 0–200 min; however, afterwards, i.e. 200 min < t < 375 min, there is no significant change. It should point out that the DGTFT offers the flexibility to tune the sensitivity through the biasing. This initial setting serves as the calibration of the device. In the next section, we show that the bottom gate biasing conditions are optimized to achieve the best operation point where the early stage detection of biofilm formation is enabled. The observed modulation of the drain current of the MZO MGTFT biosensor as a function of biofilm formation time is attributed to the electron charge transfer, resulted from the bacterial adhesion to the MZO_{nano} surface.

The bottom gate biasing voltage is used to optimize the sensor's operation point. The I–V curves in the right side of Fig. 2 shows the

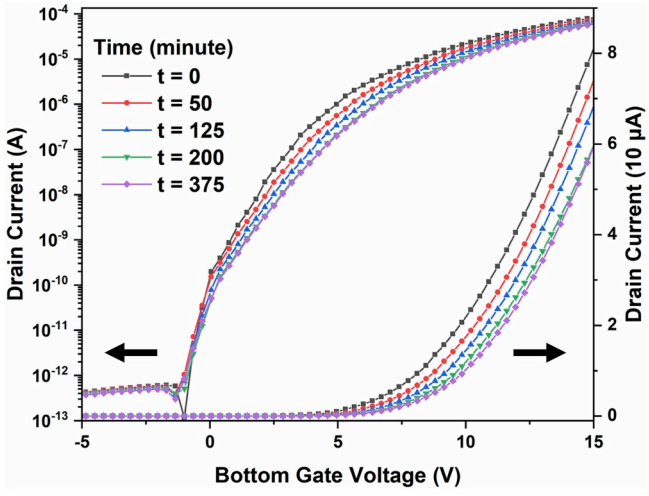

Fig. 2. The electrical transfer characteristics of the MZO DGTFT biosensor during *S. epidermidis* growth in TSB media recorded at different times. Left axis presents the drain current in logarithm scale whereas the right axis presents the same data in linear scale.

electrical characteristics as a function of incubation time plotted in linear scale, where it seems the drain current change as a function of time at any bottom gate biasing voltage between 10 V to 15 V could be used with good sensitivity. However, if the same curves are plotted in the logarithmic scale as shown in the left side of Fig. 2, we can see that there is a narrower range of bottom gate voltages that would be most suitable for sensor operation with high sensitivity. The slope of I–V transconductance plot at the triode region is much larger, and hence the current changes are more discernible. Beyond this range, the TFT enters the saturation region, where the current does not change significantly as incubation time increases, in comparison with the triode region.

3.2. Real-time monitoring of the early stage biofilm formation

We demonstrate the real time monitoring of the early stage formation of *S. epidermidis* biofilms using the MZO DGTFT sensor. Three MZO_{nano} sensing pads were prepared and the detection of *S. epidermidis* biofilms was repeated three times using the same MZO DGTFT device under the same microbial culture conditions. The *S. epidermidis* bacteria were injected at t = 0 min. For a field-effect transistor (FET) type of biosensor, the sensitivity of the device is characterized as the relative variation (*Rel. Var.*) of drain current at a certain operation condition (Rim et al., 2017). Eq. (1) was used to calculate it as a function of time:

$$Rel.\ Var. = \frac{I_D(t) - I_D(0)}{I_D(0)} \times 100\% \quad (1)$$

where $I_D(t)$ is the drain current measurement at time t, and $I_D(0)$ is the drain current measurement at the start time. The mean value and standard deviations of these relative variations were then taken from the three experiments.

As mentioned in the previous section, the bottom gate biasing voltage is used to optimize the operation point of the measurement. In the triode region of the I–V characteristic curves, the plots possess a steep slope which enhances the sensitivity; however, in the saturation region of the I–V curves, the sensitivity dramatically decreases as the slope is much smaller. To investigate the effect of bottom gate biasing voltage on sensitivity for the detection of biofilm formation, the sensor was operated at bottom gate voltage (V_{BG}) of 0 V, 2 V, 10 V, and 15 V, respectively. For each sample, the measurements were made sequentially every 25 min for a total of 375 min of the incubation time. The mean values of drain current variation as a function of incubation time and their corresponding error bars for standard deviation are presented in Fig. 3(a). The current variation at V_{BG} = 0 V is not shown in Fig. 3(a) due to large error bars (average standard deviation: 24.6%). For all four bottom gate biasing voltages, the percentage change in drain current shows significant decreasing values starting from the introduction of the bacterial culture on the MZO_{nano} sensing pad (t = 0 min) until saturation at about t = 200 min. However, it can be seen that there is a trade-off between the sensitivity and stable operation for different bottom gate biases. At V_{BG} = 15 V, the sensor exhibits smallest standard deviations indicating higher accuracy compared to the other biasing conditions. This is due to the fact that under large bottom gate bias, the TFT enters into the saturation region, where the conduction channel is fully occupied by electrons. On the other hand, the biosensor's sensitivity, which represents by the total percentage change of drain current, is higher when operated at a lower bottom gate biasing as compared to the one at V_{BG} = 15 V, which could be attributed to the steep slope in the triode region of the characteristic curve. Table 1 lists the experimental results on the slope of the transfer characteristic, maximum current change, and the average standard deviation at these four different bottom gate voltages. From the table, although the highest drain current change was found when bottom gate was grounded (i.e. V_{BG} = 0 V), the standard deviation (24.6%) is too large to make the stable and reliable operation. Therefore, V_{BG} of 2 V is selected as the optimized operation point. At this condition, the device provides high sensitivity in terms of the total percentage reduction in drain current (82.9%) and the stable operation represented by a small standard dispersion (10.1%). Fig. 3(b) represents the fitting curve of drain current variation as a function of incubation time for bottom gate bias V_{BG} of 2 V. The current change saturates at about 200 min which signifies the detection point of the onset of biofilm formation. The maximum current reduction of 82.9% is reached at incubation time t = 375 min.

Table 1
For V_{BG} = 0, 2, 10, and 15 V, the slopes of the I–V curve when t = 0 min, the maximum relative current changes, and the average standard deviations are shown in the table. A trade-off between sensitivity and dispersion is obvious with different bottom gate biases.

Bottom gate voltage V_{BG} (V)	0	2	10	15
Slope of the I–V curve when t = 0 min (V/dec)	0.44	0.93	6.35	12.62
Maximum current reduction (%)	88.0	82.9	54.9	26.4
Average standard deviation (%)	24.6	10.1	7.6	5.4

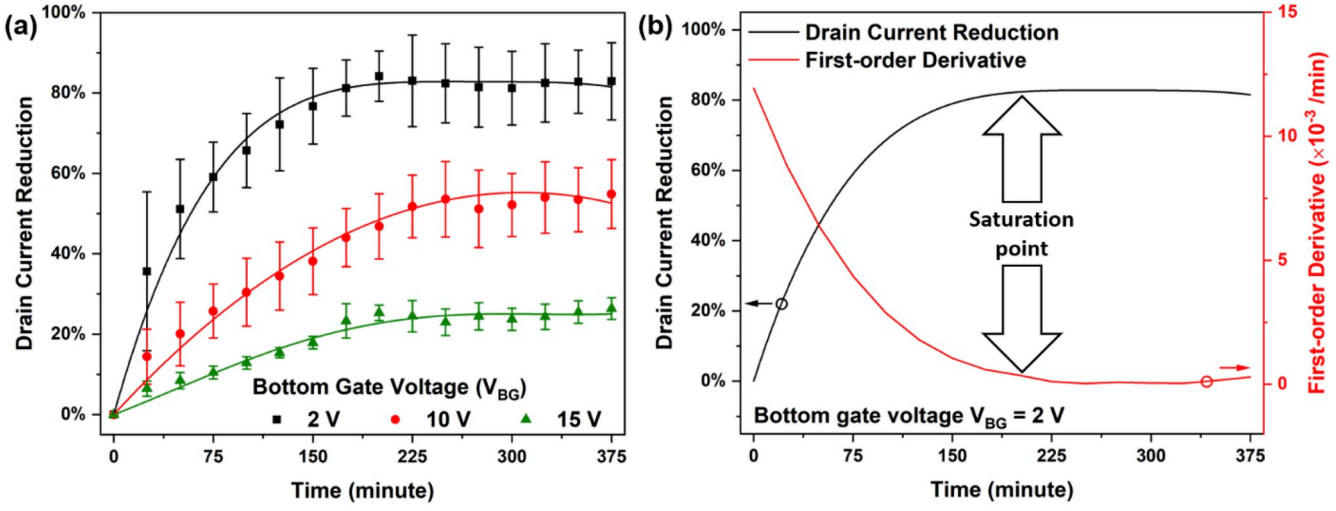

Fig. 3. (a) The relative variation of drain current reduction during *S. epidermidis* biofilm growth were extracted from the DGTFT transfer characteristics. Three different bottom gate biases (V_{BG} = 2 V, 10 V, and 15 V) are presented as a function of incubation time. No significant current variation was observed without bacterial inoculum. (b) The fitting curve of relative current reduction when V_{BG} = 2 V was plotted with its first-order derivative. The current change saturates at about t = 200 min, which indicates the end point of *S. epidermidis* biofilms early stage detection.

In Fig. 3(b) we can see that the sensor's drain current decreases rapidly as incubation time goes from t = 0 to 200 min, after which the current levels off. The decrease in drain current signifies that electron transfer has occurred between the bacterial cells and the MZO_{nano}. According to Patil et al. (2012), electrons are produced by the bacterial cells during metabolism. In the case of cell adhesion, these bacterial electrons are transferred to the electrodes or semiconducting layer such as the MZO_{nano} through a pathway called direct electron transfer (DET). The DET mechanism creates a pathway for the bacterial electron to the sensor's electrode via the bacteria's outer membrane cytochromes and conductive cell appendages. These cytochromes and conductive appendages are a product of the cell membrane due to the bacterial cell adhesion to the surface of the electrode.

The formation process of bacterial biofilms can be schematically presented by three stages: bacterial adhesion stage (early stage), bacterial expansion stage, and biofilm maturation stage, as shown in Fig. 4. As indicated in (Poortinga et al., 2001, 1999), charge transfer between bacterial cell surface and the (semi)conducting substratum surface plays an important role in the initial bacterial adhesion stage and hence influences the subsequent biofilm development process. Bacterial cell surface consists of a variety of different macromolecules including proteins which contain electrochemical active groups; particularly carboxylate functions that facilitate charge transfer. During adhesion, substratum free electrons are also present which give rise to short-range electrochemical interactions with the adhering microorganisms. The charge transfer phenomenon happening during the initial bacterial adhesion stage provides an important perspective on detecting the biofilm formation at the very early stage, as the bacterial adhesion indicates the onset of biofilm formation. Therefore, one does not have to wait until the biofilm ultimately forms. Instead, the biofilm development at the early stage can be decisively predicted by detecting the charge transfer effect using electrochemical sensors with high sensitivity such as the MZO DGTFT biosensor presented here.

While the *S. epidermidis* bacterial cells are adhering to the sensing pad and proliferate gradually, more and more negative charges are transferred from bacterial cell surface to the semiconducting MZO_{nano} sensing pad. The transferred charges introduce negative micro-bias, acting onto the MZO DGTFT's top gate. It decreases the current in the MZO channel through the electric field effect. The equivalent top gate micro-bias due to the adhered *S. epidermidis* cells can be determined from the threshold voltage shift ΔV_{TH} using Eq (2) (Baek et al., 2011).

$$V_{TG} = -\frac{C_{BI}(C_{TI} + C_{MZO})}{C_{TI}C_{MZO}}\Delta V_{TH} \tag{2}$$

where V_{TG} is the micro-bias at the top gate due to the charge transfer, ΔV_{TH} is the threshold voltage shift, C_{BI}, C_{TI}, and C_{MZO} represent the bottom gate, top gate, and the channel layer capacitance per unit area respectively. The induced charge Q at the top gate electrode was calculated using Eq. (3):

$$Q = AC_{TI}V_{TG} \tag{3}$$

where A is the area of the top gate capacitor. From Fig. 2, the threshold voltage is found to shift in the positive voltage direction by ~1.6 V from t = 0 to 375 min; therefore, approximately 10^{-12} C amount of equivalent charge is induced to the top gate-dielectric interface through the micro-bias caused by the attached bacterial cells on the MZO_{nano} sensing pad.

Both the threshold voltage change and the drain current variation could be used as the signals to represent the biofilm development process. However, the drain current varies much more significantly (~80% current variation when V_{BG} = 2 V) in comparison with the threshold voltage change (~19% threshold voltage variation). This contrast is especially obvious in the triode region of the transfer characteristics, which is selected as the operation region for sensing. Therefore, the drain current variation is chosen as the signal to represent the biofilm development process with high sensitivity.

The first-order derivative curve of the drain current reduction versus time is shown in Fig. 3(b). The DGTFT drain current dramatically decreases at the beginning of the test (large first-order derivative), resulting from the adhesion of *S. epidermidis* bacteria. Although the biofilms were still developing and far from maturation, the charge transfer effect between bacterial cell surface and substratum MZO_{nano} surface was being inhibited gradually (decreasing first-order derivative), and diminished at about 200 min. The charge transfer between the bacterial cells and the substratum is an interfacial phenomenon, and once the sensing area is covered by the interfacial adhesion cells, there will be no more charge transfer. In addition, the bacterial adhesion could induce a change in the electrical potential of substratum, and the potential change induced per adhering bacterium would decrease during the adhering process and eventually becomes zero, i.e. further charge transfer is hampered by the initial amount of charge that has been transferred. The similar phenomena has been observed and reported by Poortinga et al. (Poortinga et al., 2001, 1999). There is no lag phase exhibited by the bacterial culture and can be attributed to having the bacterial culture introduced are already in a metabolically active state and does not require time to enter cell division (Kim et al., 2012).

Crystal violet staining assay was used to verify that the biofilms indeed were formed on the MZO_{nano} sensing pads and show the time dependent long-term process of biofilm development. MZO_{nano} films were grown on the same glass substrates as the sensing pads, then they were introduced in the same bacterial biofilm incubation process. Optical images of the MZO_{nano} coated glass substrates were respectively taken at incubation time t = 0 min, 100 min, 200 min, 8 h, 16 h, and 24 h (as shown in Fig. 5(a)). For each time of culture, its absorbance values were also measured at the wavelength of 590 nm after the bound crystal violet was released (as shown in Fig. 5(b)). The absorbance measurement was repeated three times with an average standard deviation of 0.015. The value of crystal violet absorbance increases from 0.12 at t = 100 min to 0.28 at t = 200 min. Concomitantly, the current of the DGTFT

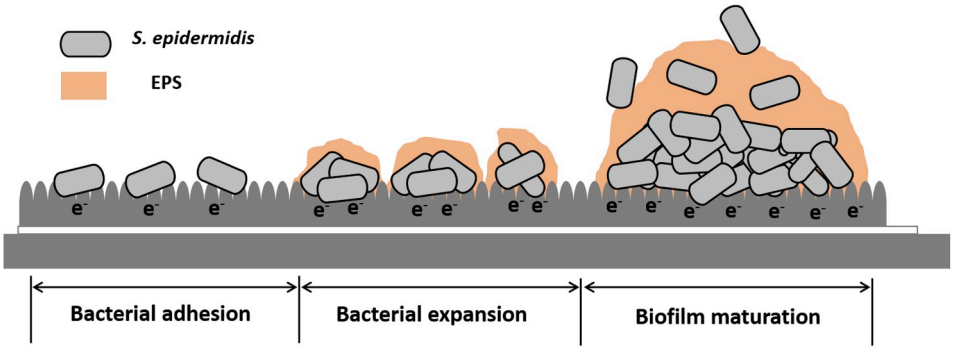

Fig. 4. The biofilm development on the nanostructure modified sensing pad is shown in three steps: 1) bacterial adhesion, 2) bacterial expansion, and 3) biofilm maturation. Electron transfer effect starts from the initial bacterial adhesion stage.

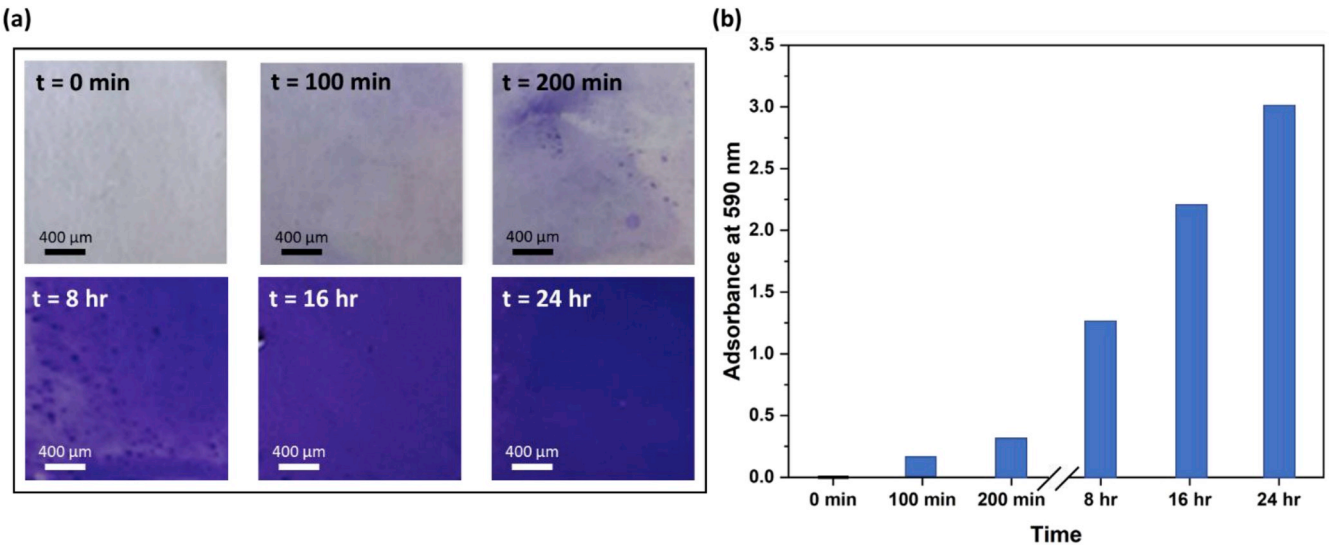

Fig. 5. (a) Optical images of crystal violet stained *S. epidermidis* biofilms on MZO_{nano} films, recorded at 0 min, 100 min, 200 min, 8 h, 16 h, and 24 h. (b) Quantification of the biofilm formation process at different times of culture by measuring the absorbance at 590 nm. (For interpretation of the references to colour in this figure legend, the reader is referred to the Web version of this article.)

biosensor decreases from 6.60×10^{-9} A at t = 100 min to 3.00×10^{-9} A at t = 200 min. Therefore, the statistical correlation between these two results obtained by different techniques is achieved. From the biosensor standpoint, t = 200 min is the moment when the signal starts to saturate, indicating that cellular adhesion has taken place. It is defined as the onset of biofilm formation. However, at 200 min, the crystal violet staining assay results show that tiny bacterial microcolonies just start to form at the sites of adhesion as shown in Fig. 5(a). Afterwards, with the EPS production and bacterial cell proliferation, it took approximately 24 h to develop into the matured biofilms.

Initial bacterial adhesion is the onset of biofilm formation, and it is detected no longer than 200 min by using the novel MZO DGTFT biosensor. Crystal violet staining assay shows bacterial microcolonies just form up at 200 min and the biofilms get matured at approximately 24 h. Thus, the trend of biofilm formation has been predicated at its early stage, allowing medical professionals to act ahead of time to inhibit the subsequent biofilm formation.

3.3. Effects of nanostructures (MZO_{nano} vs ZnO_{nano}) on sensing performance

The effects of DGTFT using the different nanostructures as the extended sensing gate are studied. The extended sensing gates are made up of MZO_{nano} and ZnO_{nano}, respectively. It is well known that ZnO can alloy with MgO to form the ternary compound $Mg_xZn_{1-x}O$ to extend the energy bandgap. The direct energy bandgap of wurtzite-structured $Mg_xZn_{1-x}O$ can be tuned up to ~4.0 eV (x = 0.34). The energy bandgap of $Mg_xZn_{1-x}O$ follows Vegard's law (Zhong and Lu, 2011) Eq. (4):

$$E_g(Mg_xZn_{1-x}O) = xE_g(MgO) + (1-x)E_g(ZnO) \quad (4)$$

where $E_g(Mg_xZn_{1-x}O)$, $E_g(MgO)$ and $E_g(ZnO)$ are the energy bandgaps of MZO, MgO and ZnO, respectively. For small x value, the $E_g(Mg_xZn_{1-x}O)$ can be estimated by the linear approximation:

$$E_g(Mg_xZn_{1-x}O) = E_g(ZnO) + bx \quad (5)$$

where b is a constant number from fitting.

In this work, the energy bandgaps of MZO and ZnO are experimentally determined by optical absorption measurements. Near the absorption edge, the relationship between the absorption coefficient α and the photon energy $h\nu$ is given by Eq. (6):

$$\alpha \propto (h\nu - E_g)^{1/2} \quad (6)$$

where α is the absorption coefficient, $h\nu$ is the photon energy, and E_g is the energy bandgap. By measuring α^2 versus $h\nu$ respectively for $Mg_xZn_{1-x}O$ (MZO) and ZnO, and then curve fitting, the energy bandgaps E_g can be determined (Duan et al., 2012). The absorption spectra of ZnO and MZO were acquired at room temperature using the Beckman DU 530 UV–visible spectrometer. Fig. 6(a) shows the measured curves of α^2 versus $h\nu$, where the bandgaps of ZnO and $Mg_xZn_{1-x}O$ (MZO) are determined to be 3.26 eV and 3.36 eV, respectively. The linear relationship in Eq. (5) is then used to decide the x value in $Mg_xZn_{1-x}O$ to be ~0.04 (4%), where $b \approx 2.5$.

S. epidermidis biofilms were cultured on the bare sensing pads (Cr/Au coated glass, i.e. metal/glass), pure ZnO nanostructures (ZnO_{nano} on metal/glass), and MZO nanostructures (MZO_{nano} on metal/glass) modified sensing pads for 60 min under the same conditions, respectively. These three different sensing pads were then separately connected to the top gate of the same MZO DGTFT. The electrical measurements were performed for each of them. The bottom gate voltage was set at $V_{BG} = 2$ V, and the relative drain current reductions were obtained in comparison with the same type of pad without biofilm incubation. The same experiment was repeated three times for each type of the sensing materials. Shown in Fig. 6(b) are the mean values of the drain current reduction and the standard deviation error bars of the DGTFT with each sensing pad, respectively. The bare sensing pad without nanostructure coating essentially failed bacterial measurements due to low sensitivity while both devices with the ZnO_{nano} or MZO_{nano} sensing pad are able to detect the drain current reduction; 19% and 66%, respectively.

From the comparison, it is clear that the modification of sensing surface with the ZnO_{nano} and MZO_{nano} can achieve higher sensitivity; therefore, enabling the early stage detection of biofilm formation. The surface roughness impact on the biofilm formation can be explained by two factors. First, the bacteria prefer to start adhesion at somewhere sheltered from shear forces so that they have time to change from reversible to irreversible attachment (Teughels et al., 2006). Second, the effective area for adhesion is significantly increased due to the roughening of surface. In addition, the ZnO_{nano} and MZO_{nano} underwent UV light illumination and thus exhibited super-hydrophilicity (Zhang et al., 2007b). The super-hydrophilicity enables less liquid sample

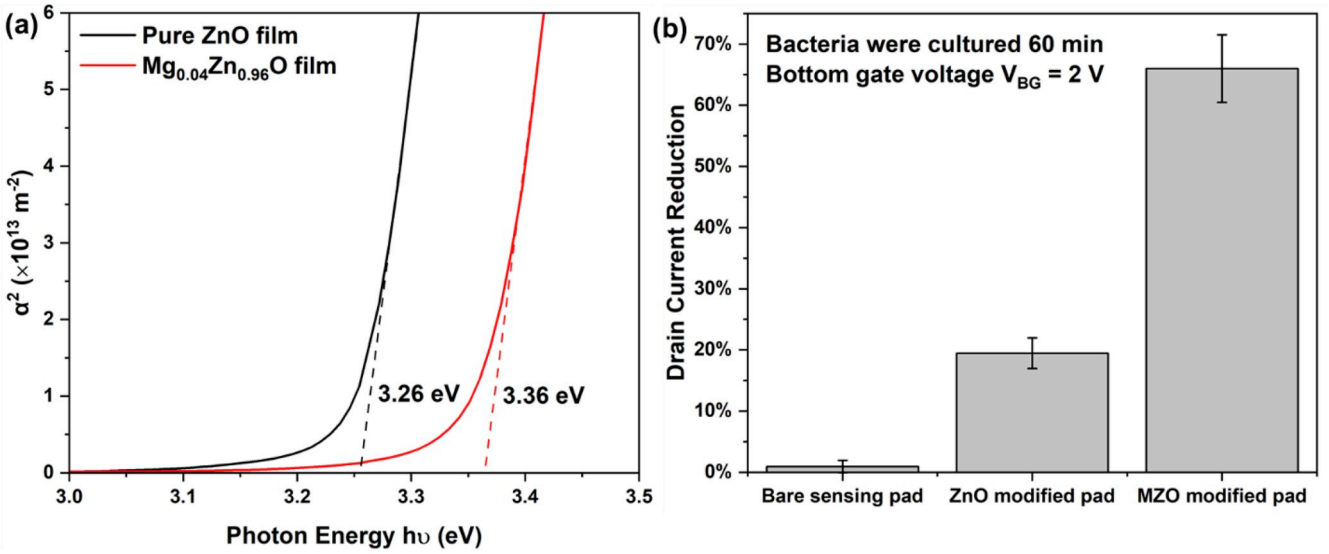

Fig. 6. (a) The optical absorption measurements were performed for both ZnO and MZO films on glass substrates, respectively. The absorption coefficient squares α^2 are plotted against photon energy hυ for ZnO and MZO films. The bandgaps of ZnO and MZO films are determined to be 3.26 eV and 3.36 eV, respectively, which indicates the x value in $Mg_xZn_{1-x}O$ to be ~0.04 (4%). (b) S. epidermidis biofilms were respectively incubated on bare sensing pads, ZnO_{nano} modified pads, and MZO_{nano} modified pads for 60 min. The same MZO DGTFT was used to conduct the experiments. Bottom gate voltage was set at 2 V. The relative variations of drain current reduction were obtained comparing with the same type of pad without bacteria incubation.

consumption and higher sensitivity.

The above comparative studies also demonstrate that the sensing pad with the MZO_{nano} modification offers much high sensitivity over the pure ZnO_{nano} counterpart. ZnO would release Zn^{2+} ions in acidic environment, and that the Zn^{2+} ions are toxic to bacterial cells (Nel et al., 2009). The Zn^{2+} ion formation proceeds as follows Eq. (7):

$$ZnO + 2H^+ \rightarrow Zn^{2+} + OH^- + H^+ \rightarrow Zn^{2+} + H_2O \quad (7)$$

where, the Zn–O bond in ZnO_{nano} can be easily attacked by hydronium ions in acidic solutions. In our case, as the biofilms secreted by *S. epidermidis* is acidic with a pH value between 4 - 5 (Stewart et al., 2017), the chemical reaction holds. The use of pure ZnO_{nano} sensing pad could decrease the sensitivity of the biosensor as the Zn^{2+} ions migrating into the growth medium and thus the cells are killed to some extent. By adding small composition of MgO (~4%) into pure ZnO to form the MZO, Zn^{2+} ions are significantly reduced due to the stronger bonding between Mg and the metal oxide surface compared to Zn. We observed similar phenomenon in (Reyes et al., 2017). In this work, MZO_{nano} is chosen as the optimized sensing material over pure ZnO_{nano} to reduce the toxicity to *S. epidermidis*; therefore, improve the device sensitivity.

4. Conclusion

A biosensor consisting of an MZO DGTFT and an extended MZO nanostructure modified sensing gate was developed for the early stage detection of *S. epidermidis* bacterial biofilm formation. The $Mg_xZn_{1-x}O$ (x = 0.04) nanostructures with properly controlled surface morphology and wettability provide the giant effective surface area and preferred conditions for bacteria adhesion, concomitantly reduce the biotoxicity to *S. epidermidis* bacteria by suppressing Zn^{2+} ions in the culture medium. The extended sensing gate design isolated the bacterial incubation from the DGTFT device, and thus allowed the continuous and dynamic detection in aqueous environment. The dual gate design of the MZO DGTFT possess the biasing flexibility and stable operation, enabling the device to operate at the proper characteristic region. The bottom gate biasing voltage V_{BG} = 2 V was selected to achieve high sensitivity and stable operation. A drain current change of ~80% (with an average standard deviation of ~10%) is achieved after ~200 min of *S. epidermidis* bacteria culturing, which signified the detection point for the onset of biofilm formation. In comparison, the crystal violet staining assay shows the matured biofilms would take approximately 24 h to form. This MZO DGTFT biosensor is promising in clinical applications as it could alert medical professionals to treat bacterial infections promptly and more effectively.

Declaration of competing interest

The authors declare that they have no known competing financial interests or personal relationships that could have appeared to influence the work reported in this paper.

CRediT authorship contribution statement

Guangyuan Li: Conceptualization, Methodology, Investigation, Data curation, Writing - original draft, Formal analysis, Visualization. **Yifan Wu:** Methodology, Investigation. **Yuxuan Li:** Methodology, Investigation. **Yuzhi Hong:** Methodology, Validation, Investigation. **Xilin Zhao:** Resources, Conceptualization, Supervision. **Pavel Ivanoff Reyes:** Conceptualization, Supervision, Formal analysis, Writing - review & editing, Visualization. **Yicheng Lu:** Conceptualization, Supervision, Resources, Writing - review & editing.

Acknowledgements

This work is supported in part by the Rutgers TechAdvance(TM) Early Technology Development Grant # 205719.

References

Astorga, S.E., Hu, L.X., Marsili, E., Huang, Y., 2019. ChemElectroChem 6, 4674–4680.
Baek, G., Abe, K., Kuo, A., Kumomi, H., Kanicki, J., 2011. IEEE Trans. Electron Devices 58, 4344–4353.
Becerro, S., Paredes, J., Mujika, M., Pérez Lorenzo, E., Arana, S., 2016. IEEE Sens. J. 16, 1856–1864.
Bryers, J.D., 2008. Biotechnol. Bioeng. 100, 1–18.
Cao, Y., Galoppini, E., Reyes, P.I., Duan, Z., Lu, Y., 2012. Langmuir 28, 7947–7951.
Chen, M.Y., Chen, M.J., Lee, P.F., Cheng, L.H., Huang, L.J., Lai, C.H., Huang, K.H., 2010. Biochem. Eng. J. 53, 121–130.
Duan, Z., Du Pasquier, A., Lu, Y., Xu, Y., Garfunkel, E., 2012. Sol. Energy Mater. Sol. Cells 96, 292–297.
Van Epps, J.S., Younger, J.G., 2016. Shock 46, 597–608.

Hall-Stoodley, L., Costerton, J.W., Stoodley, P., 2004. Nat. Rev. Microbiol. 2, 95–108.
Hong, W.C., Ku, C.J., Li, R., Abbaslou, S., Reyes, P., Wang, S.Y., Li, G., Lu, M., Sheng, K., Lu, Y., 2016. Sci. Rep. 6.
International Trade Administration, 2016. 2016 ITA Medical Devices Top Markets Report.
Khatoon, Z., McTiernan, C.D., Suuronen, E.J., Mah, T.F., Alarcon, E.I., 2018. Heliyon 4, e01067.
Kiers, P.J.M., Bos, R., van der Mei, H.C., Busscher, H.J., 2001. Microbiology 147, 757–762.
Kim, Y.W., Meyer, M.T., Berkovich, A., Subramanian, S., Iliadis, A.A., Bentley, W.E., Ghodssi, R., 2016. Sens. Actuators, A Phys. 238, 140–149.
Kim, Y.W., Sardari, S.E., Meyer, M.T., Iliadis, A.A., Wu, H.C., Bentley, W.E., Ghodssi, R., 2012. Sens. Actuators B Chem. 163, 136–145.
Ku, C.-J., Duan, Z., Reyes, P.I., Lu, Y., Xu, Y., Hsueh, C.-L., Garfunkel, E., 2011. Appl. Phys. Lett. 98, 123511.
Ku, C.J., Hong, W.C., Mohsin, T., Li, R., Duan, Z., Lu, Y., 2015. IEEE Electron. Device Lett. 36, 914–916.
Li, R., Li, G., Hong, W.C., Reyes, P.I., Tang, K., Yang, K., Wang, S.Y., Ye, H., Li, Y., Zhang, L., Kisslinger, K., Lu, Y., 2018. Smart Mater. Struct. 27.
Liu, L., Xu, Y., Cui, F., Xia, Y., Chen, L., Mou, X., Lv, J., 2018. Biosens. Bioelectron. 112, 86–92.
Lu, Y., Chen, Y., Zhang, Z., 2011. Multifunctional biosensor based on ZnO nanostructures. U.S. Patent 7,989,851..
Muthukumar, S., Sheng, H., Zhong, J., Zhang, Z., Emanetoglu, N.W., Lu, Y., 2003. IEEE Trans. Nanotechnol. 2, 50–54.
Nel, A.E., Mädler, L., Velegol, D., Xia, T., Hoek, E.M.V., Somasundaran, P., Klaessig, F., Castranova, V., Thompson, M., 2009. Nat. Mater. 8, 543–557.
Norton, T.A., Thompson, R.C., Pope, J., Veltkamp, C.J., Banks, B., Howard, C.V., Hawkins, S.J., 1998. Aquat. Microb. Ecol. 16, 199–204.
Paredes, Jacobo, Becerro, S., Arana, S., 2014a. J. Microbiol. Methods 100, 77–83.
Paredes, J., Becerro, S., Arana, S., 2014b. Sens. Actuators B Chem. 195, 667–676.
Paredes, J., Becerro, S., Arizti, F., Aguinaga, A., Del Pozo, J.L., Arana, S., 2012. Biosens. Bioelectron. 38, 226–232.
Paredes, J., Becerro, S., Arizti, F., Aguinaga, A., Del Pozo, J.L., Arana, S., 2013. Sens. Actuators B Chem. 178, 663–670.
Patil, S.A., Hägerhäll, C., Gorton, L., 2012. Bioanal. Rev. 4, 159–192.
Peeters, E., Nelis, H.J., Coenye, T., 2008. J. Microbiol. Methods 72, 157–165.
Pires, L., Sachsenheimer, K., Kleintschek, T., Waldbaur, A., Schwartz, T., Rapp, B.E., 2013. Biosens. Bioelectron. 47, 157–163.
Poortinga, A.T., Bos, R., Busscher, H.J., 1999. J. Microbiol. Methods 38, 183–189.
Poortinga, A.T., Bos, R., Busscher, H.J., 2001. Biophys. Chem. 91, 273–279.
Del Pozo, J.L., Rouse, M.S., Mandrekar, J.N., Sampedro, M.F., Steckelberg, J.M., Patel, R., 2009. Antimicrob. Agents Chemother. 53, 35–40.
Reyes, P.I., Duan, Z., Lu, Y., Khavulya, D., Boustany, N., 2013. Biosens. Bioelectron. 41, 84–89.
Reyes, P.I., Ku, C.J., Duan, Z., Lu, Y., Solanki, A., Lee, K.B., 2011. Appl. Phys. Lett. 98, 1–4.
Reyes, P.I., Yang, K., Zheng, A., Li, R., Li, G., Lu, Y., Tsang, C.K., Zheng, S.X.F., 2017. Biosens. Bioelectron. 93, 189–197.
Reyes, P.I., Zhang, Z., Chen, H., Duan, Z., Zhong, J., Saraf, G., Lu, Y., Taratula, O., Galoppini, E., Boustany, N.N., 2009. IEEE Sens. J. 9, 1302–1307.
Rim, Y.S., Chen, H., Zhu, B., Bae, S.-H., Zhu, S., Li, P.J., Wang, I.C., Yang, Y., 2017. Adv. Mater. Interfaces 4, 1700020.
Seok, M.J., Choi, M.H., Mativenga, M., Geng, D., Kim, D.Y., Jang, J., 2011. IEEE Electron. Device Lett. 32, 1089–1091.
Seok, M.J., Mativenga, M., Geng, D., Jang, J., 2013. IEEE Trans. Electron Devices 60, 3787–3793.
Spijkman, M., Smits, E.C.P., Blom, P.W.M., De Leeuw, D.M., Bon Saint Côme, Y., Setayesh, S., Cantatore, E., 2008. Appl. Phys. Lett. 92, 1–4.
Stewart, E.J., Payne, D.E., Ma, T.M., Scott VanEpps, J., Boles, B.R., Younger, J.G., Solomon, M.J., 2017. Appl. Environ. Microbiol. 83, 1–14.
Tai, Y.H., Chiu, H.L., Chou, L.S., 2012a. Solid State Electron. 72, 67–72.
Tai, Y.H., Chou, L.S., Chiu, H.L., Chen, B.C., 2012b. IEEE Electron. Device Lett. 33, 393–395.
Taratula, O., Galoppini, E., Wang, D., Chu, D., Zhang, Z., Chen, H., Saraf, G., Lu, Y., 2006. J. Phys. Chem. B 110, 6506–6515.
Teughels, W., Van Assche, N., Sliepen, I., Quirynen, M., 2006. Clin. Oral Implant. Res. 17, 68–81.
Zhang, Zheng, Chen, H., Zhong, J., Chen, Y., Lu, Y., 2007a. Proc. IEEE Int. Freq. Control Symp. Expo. 545–549.
Zhang, Z., Chen, H., Zhong, J., Saraf, G., Lu, Y., 2007b. J. Electron. Mater. 36, 895–899.
Zhong, J., Lu, Y., 2011. ZnO-based ultraviolet detectors. In: Zinc Oxide Materials for Electronic and Optoelectronic Device Applications. John Wiley & Sons, Ltd, Chichester, UK, pp. 287–329.